Image and Vision Computing 28 (2010) 298–306

Contents lists available at ScienceDirect

Image and Vision Computing

journal homepage: www.elsevier.com/locate/imavis

Adaptive total variation denoising based on difference curvature

Qiang Chen [a,*], Philippe Montesinos [b], Quan Sen Sun [a], Peng Ann Heng [c,d], De Shen Xia [a]

[a] The School of Computer Science and Technology, Nanjing University of Science and Technology, Xiao Lingwei 200#, Nanjing, Jiangsu 210094, China
[b] EMA-EERIE, LGI2P, Parc Scientifique G. Besse, Nimes, France
[c] Shenzhen Institute of Advanced Integration Technology, Chinese Academy of Sciences, The Chinese University of Hong Kong, Shenzhen, China
[d] Department of Computer Science & Engineering, The Chinese University of Hong Kong, Hong Kong, china

ARTICLE INFO

Article history:
Received 21 July 2007
Received in revised form 11 May 2008
Accepted 20 April 2009

Keywords:
Image denoise
Total variation
Difference curvature
Staircase effect
Loss of details

ABSTRACT

Image denoising methods based on gradient dependent regularizers such as Rudin et al.'s total variation (TV) model often suffer the staircase effect and the loss of fine details. In order to overcome such drawbacks, this paper presents an adaptive total variation method based on a new edge indicator, named difference curvature, which can effectively distinguish between edges and ramps. With adaptive regularization and fidelity terms, the new model has the following properties: at object edges, the regularization term is approximate to the TV norm in order to preserve the edges, and the weight of the fidelity term is large in order to preserve details; in flat and ramp regions, the regularization term is approximate to the L2 norm in order to avoid the staircase effect, and the weight of the fidelity term is small in order to strongly remove the noise. Comparative results on both synthetic and natural images demonstrate that the new method can avoid the staircase effect and better preserve fine details.

1. Introduction

The degradation of an image is usually unavoidable during its acquisition, and perhaps the most fundamental image restoration problem is denoising. It forms a significant preliminary step in many machine vision tasks, such as object detection and recognition. A major concern in designing image denoising models is to preserve important image features, such as edges, while removing noise. Variational [1–4] and PDE [5–11] based models have been widely used over the past decades for image denoising with edge preservation. A classical variational denoising method is the total variation minimizing process of Rudin–Osher–Fatemi (ROF) [1]. The ROF model seeks the minimal energy of an energy functional comprised of the TV norm of the image u and the fidelity of this image to the noisy input image u_0:

$$E_{TV} = \int_{\Omega} \left(|\nabla u| + \frac{1}{2}\lambda (u - u_0)^2 \right) dx\, dy \tag{1}$$

Here, Ω denotes the image domain, and $\lambda > 0$ is a weight parameter. The TV norm $\int_{\Omega} |\nabla u|$ is a regularizing term to remove the noise, and $\int_{\Omega}(u-u_0)^2$ is a fidelity term.

Although the ROF model can reduce oscillations and regularize the geometry of level sets without penalizing discontinuities, it possesses some properties which may be undesirable under some circumstances [12], such as staircasing and loss of texture. Addressing the drawbacks of the original ROF model, many improved TV models have been proposed. In order to compensate for the loss of contrast and textures, an iterative regularization method on the ROF model was proposed by Osher et al. [13], and the squared L2 norm in the fidelity term in (1) was replaced by the L1 norm in [14,15]. In [2] a spatially varying fidelity term was adopted to better preserve fine scale features. In [16], Esedoglu and Osher introduced and studied anisotropic version of the ROF model to privilege certain edge directions. Staircasing is one of the potential drawbacks of the ROF model. The TV model is borderline convex: its dependence on image gradients is linear at infinity. This feature preserves edges well, but the images resulting of the application in the presence of noise are often piecewise constant, thus the finer details in the original image may not be recovered satisfactorily and that ramps (affine regions) will give stairs (piecewise constant regions). A natural approach to overcome the staircase effect is to make the ROF model more convex in regions of moderate gradient (away from the edges). A functional designed to accomplish this was proposed by Blomgren et al. [3,17]. It has the form

$$\int_{\Omega} |\nabla u|^{P(|\nabla u|)}\, dx + \lambda \int_{\Omega} (u - f)^2\, dx \tag{2}$$

Here, the function $P(s) : \Re^+ \to [1,2]$ is chosen to be monotonically decreasing from 2 to 1. Bouman and Sauer [18] presented a generalized Gaussian Markov random field (GGMRF) for edge-preserving MAP estimation, which satisfies several desirable analytical and computational properties for MAP estimation, including continuous dependence of the estimate on the data, invariance of the character of solutions to scaling of data, and a solution which lies at the

* Corresponding author. Tel.: +86 025 84315142.
E-mail address: chen2qiang@163.com (Q. Chen).

0262-8856/$ - see front matter © 2009 Elsevier B.V. All rights reserved.
doi:10.1016/j.imavis.2009.04.012

Table 1
Behavioral analysis of three curvatures, where 'L' and 'S' denote 'large' and 'small', respectively.

	Difference curvature (D)	Mean curvature (M)	Gaussian curvature (G)
Edge	L	L	S
Flat region	S	S	S
Ramp region	S	S	S
Isolated noise	S	L	L

unique global minimum of the a posteriori log-likelihood function. Another approach to preventing staircasing is to introduce the higher order derivatives into the energy [3,4,10,11,19–21]. Although the high order PDEs can preserve ramps without penalizing sharp edges, the mathematical problem is much more challenging. In order to take the advantage of the ROF filter and the fourth-order filter since it is able to preserve edges while avoiding the staircase effect, the combined models of both filters were proposed by Lysaker and

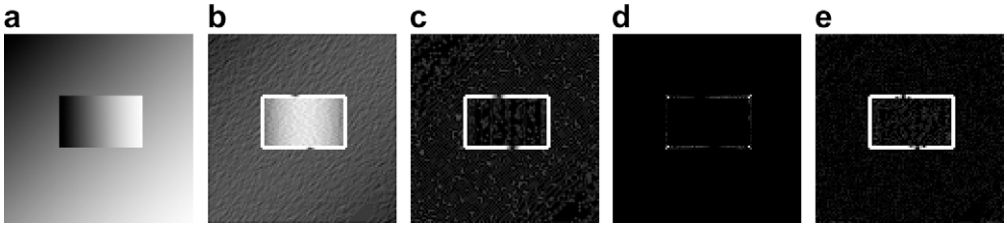

Fig. 1. Comparison of the effect on a ramp image. (a) Original image. (b) Effect of the gradient. (c) Effect of the mean curvature. (d) Effect of the Gaussian curvature. (e) Effect of the difference curvature.

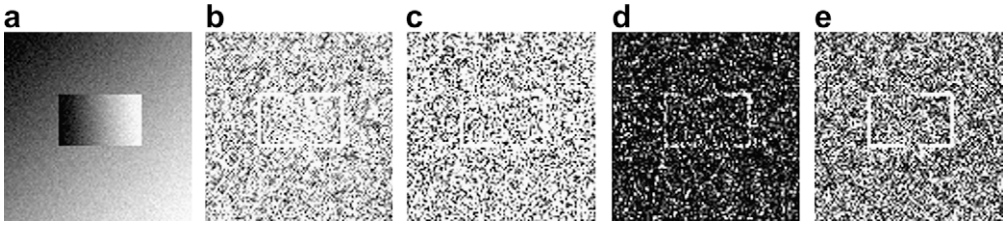

Fig. 2. Comparison of the effect on a noisy ramp image. (a) Noisy image. (b) Effect of the gradient. (c) Effect of the mean curvature. (d) Effect of the Gaussian curvature. (e) Effect of the difference curvature.

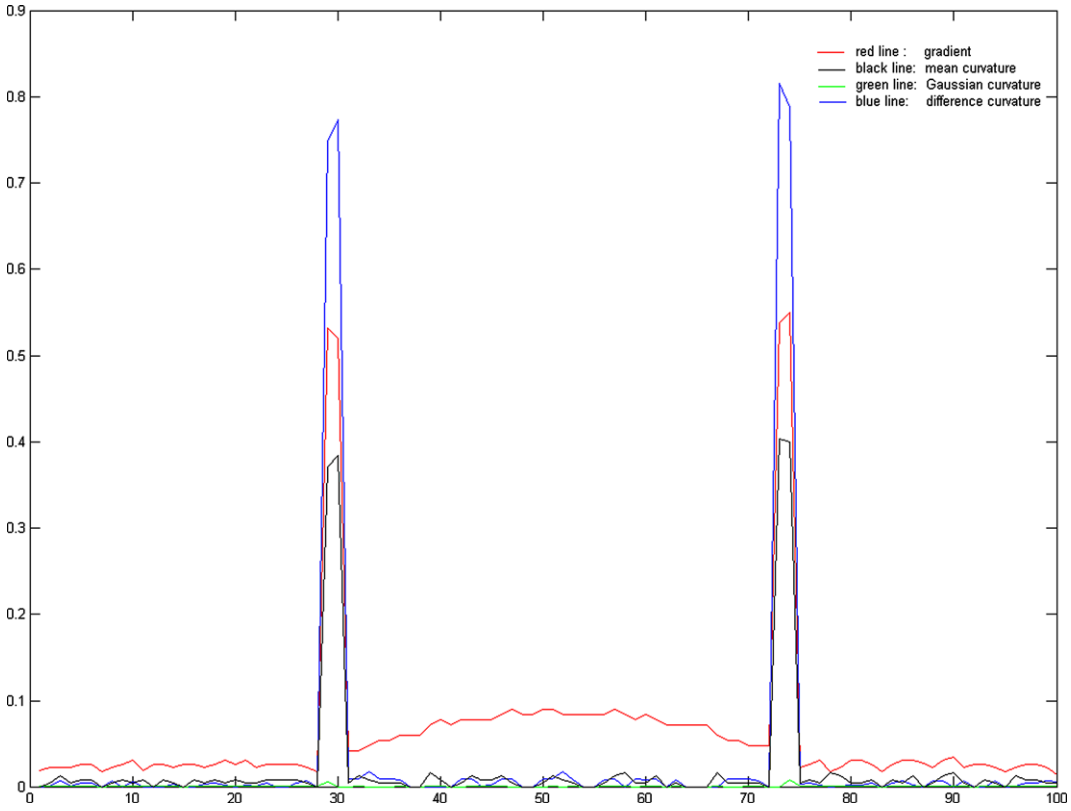

Fig. 3. One line profile of Fig. 1(b)–(e).

Tai [22] and Li et al. [23]. In order to preserve details and avoid staircasing, several total variation based filters with convex variational penalty functions were introduced, such as the edge-flat-grey (EFG) scale filtering [24] and Gauss-TV filtering [25].

In this paper, we propose an *adaptive TV* (ATV) model based on a new edge indictor, which can effectively distinguish between ramps and edges. In the ATV model, the regularization term and the fidelity term are adaptive, which have the following properties: (1) at object edges, the regularization term is approximate to the TV norm in order to preserve the edges, and the weight of the fidelity term is large in order to preserve details; (2) in flat and ramp regions, the regularization term is approximate to the L2 norm in order to avoid the staircase effect, and the weight of the fidelity term is small in order to strongly remove the noise.

The remainder of this paper is organized as follows: Section 2 presents the new edge indicator, difference curvature. Based on the difference curvature, the ATV model is presented in Section 3. Section 4 compares and analyzes the performance of our model with those of some other denoising methods. Finally, conclusions are drawn in Section 5.

2. New edge indicator

2.1. Definition

Traditional edge indicators based on the image gradient cannot effectively distinguish between edges and ramps. The second derivatives can effectively distinguish edges and ramps for one-dimensional signal [4]. Similarly, in the two-dimensional case of images, the new edge indicator proposed in this paper is

$$D = \|u_{\eta\eta}| - |u_{\xi\xi}\| \tag{3}$$

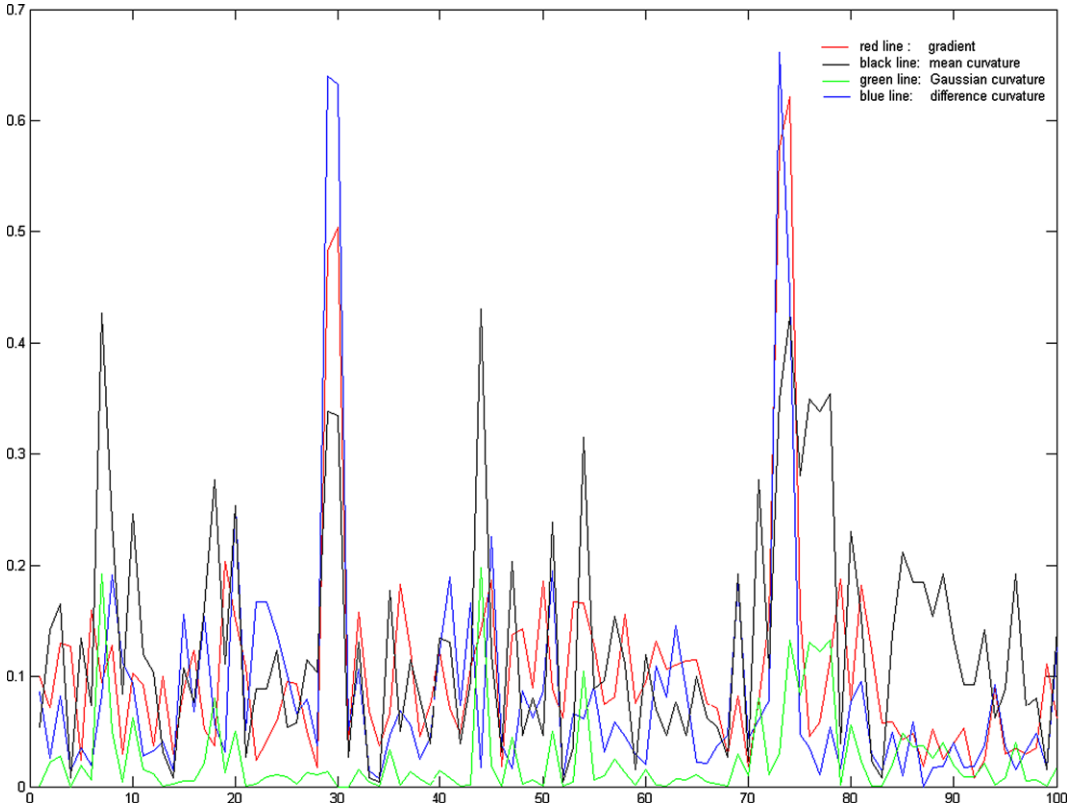

Fig. 4. One line profile of Fig. 2(b)–(e).

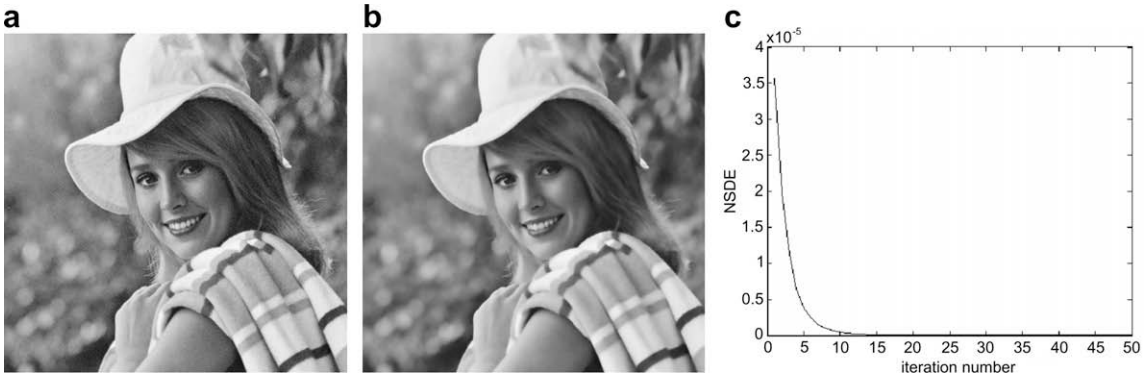

Fig. 5. Denoising result of the Elaine image. (a) Original image. (b) Denoising result. (c) Normalized step difference energy for our model.

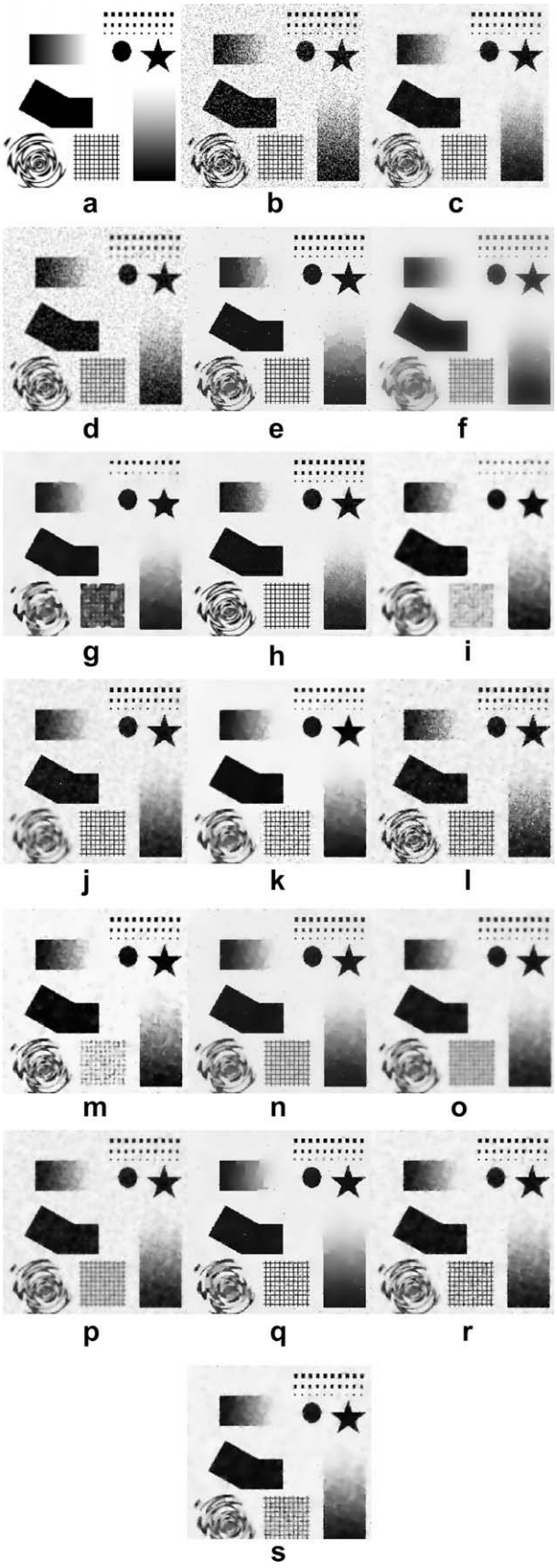

Fig. 6. Comparison of the effect on a synthetic image. (a) Original image. (b) Noisy image (additive Gaussian white noise, SNR = 7.6 db). (c) Bilateral filtering. (d) GCDD. (e) PM. (f) Nonlinear complex diffusion. (g) Adaptive smoothing. (h) NL-means. (i) LYNF. (j) Robust anisotropic diffusion. (k) Adaptive TV. (l) Fourth-order PDEs. (m) TV. (n) TV2&4. (o) EFG. (p) Gauss-TV. (q) Nonlinear diffusion filtering. (r) ATV. (s) ATV-TV.

where $u_{\eta\eta} = \frac{u_x^2 u_{xx} + 2u_x u_y u_{xy} + u_y^2 u_{yy}}{u_x^2 + u_y^2}$ and $u_{\xi\xi} = \frac{u_y^2 u_{xx} - 2u_x u_y u_{xy} + u_x^2 u_{yy}}{u_x^2 + u_y^2}$ represent the second derivatives in the direction of the gradient ∇u and in the direction perpendicular to ∇u, respectively, and the operator $|\cdot|$ denotes the absolute value. In this paper, we call the new edge indicator D *difference curvature*. The behavioral analysis of the new edge indicator is as follows:

(a) For edges, $|u_{\eta\eta}|$ is large and $|u_{\xi\xi}|$ is small, so $D$is large.
(b) For flat and ramp regions, $|u_{\eta\eta}|$ and $|u_{\xi\xi}|$ are both small, so D is small.
(c) For isolated noise, $|u_{\eta\eta}|$ and $|u_{\xi\xi}|$ are both large and almost equal, so D is small.

According to the analysis above, edges can be distinguished from flat and ramp regions based on the value of D.

2.2. Comparison between difference curvature and other curvatures

The mean curvature is the average of $u_{\eta\eta}$ and $u_{\xi\xi}$, which can be written as

$$M = \frac{(u_{\eta\eta} + u_{\xi\xi})}{2} \tag{4}$$

The Gaussian curvature is the product of $u_{\eta\eta}$ and $u_{\xi\xi}$, which can be written as

$$G = u_{\eta\eta} \cdot u_{\xi\xi} \tag{5}$$

Table 1 shows the behavioral analysis of the three curvatures, i.e. difference curvature, mean curvature and Gaussian curvature. From Table 1, it can be observed that the mean curvature cannot distinguish between edges and isolated noise, therefore the image denoising based on mean curvature cannot preserve edges. The Gaussian curvature can distinguish isolated noise from the edge, flat and ramp regions, but our empirical studies indicate that it does not work effectively in the presence of severe noise. The difference curvature proposed above can distinguish edges from flat and ramp regions and isolated noise.

Figs. 1 and 2 show the comparisons of the effect on a ramp image consisting of 100 × 100 pixels and a noisy ramp image, respectively. In order to facilitate the display of their difference, Figs. 1(b)–(e) and 2(b)–(e) are normalized to be within $\left[0, \frac{10 \cdot e}{\max(e)}\right]$, where $e \in \{\nabla u, D, |M|, |G|\}$. Figs. 3 and 4 show one line profile of the 50th rows of Figs. 1(b)–(e) and 2(b)–(e), respectively. From Figs. 1–4, it can be seen that the mean curvature and the difference curvature have a greater capability in distinguishing edges and ramps than

Table 2
SNR results of Fig. 6 (unit: db).

Figures	6(b)	6(c)	6(d)	6(e)	6(f)	6(g)	6(h)	6(i)	6(j)
SNR	7.6441	11.6903	8.4246	12.1084	7.2685	6.9972	13.4898	7.1239	11.2362
Figures	6(k)	6(l)	6(m)	6(n)	6(o)	6(p)	6(q)	6(r)	6(s)
SNR	11.9273	10.6487	9.3147	10.065	7.7815	8.6629	11.6853	10.787	10.266

Table 3
Mean structural similarity (MSSIM) of Fig. 6. The MSSIM is between 0 and 1 with a score of 1 being given only if the denoised image is exactly equivalent to the original image.

Figures	6(b)	6(c)	6(d)	6(e)	6(f)	6(g)	6(h)	6(i)	6(j)
MSSIM	0.3378	0.6276	0.4040	0.7858	0.7213	0.7287	0.7575	0.6520	0.7189
Figures	6(k)	6(l)	6(m)	6(n)	6(o)	6(p)	6(q)	6(r)	6(s)
MSSIM	0.8244	0.6460	0.7494	0.7853	0.7237	0.6850	0.8364	0.7702	0.8002

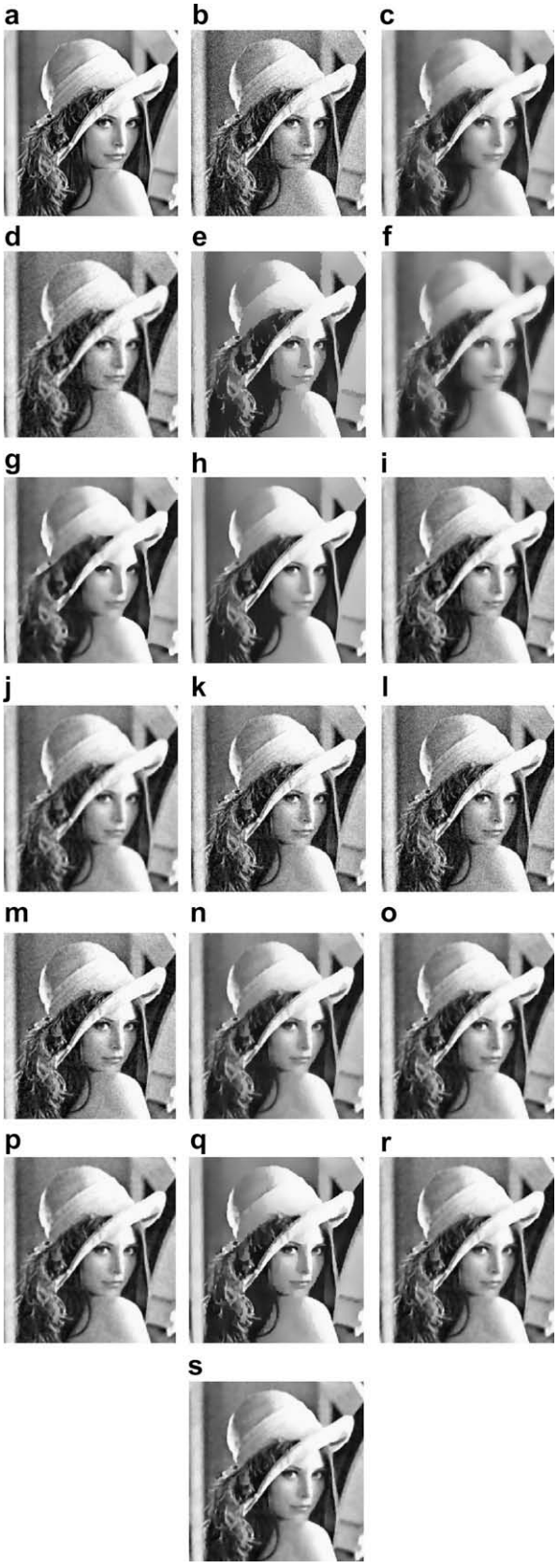

Fig. 7. Comparison of the effect on a natural image. (a) Original image. (b) Noisy image (additive Gaussian white noise, SNR = 12.4 db). (c) Bilateral filtering. (d) GCDD. (e) PM. (f) Nonlinear complex diffusion. (g) Adaptive smoothing. (h) NL-means. (i) LYNF. (j) Robust anisotropic diffusion. (k) Adaptive TV. (l) Fourth-order PDEs. (m) TV. (n) TV2&4. (o) EFG. (p) Gauss-TV. (q) Nonlinear diffusion filtering. (r) ATV. (s) ATV-TV.

the image gradient, but in the noisy image the difference curvature is more noise-immune than the gradient and the mean curvature. For the Gaussian curvature, similarly with isolated noise, the values at corners are large, therefore the denoising based on the Gaussian curvature cannot preserve corners. Since the gradient difference between edges and ramps is not significant, anisotropic diffusions based on the image gradient are prone to cause the staircase effect in ramp regions.

In order to avoid staircase effects and better preserve fine details, we present a natural way to improve the TV model based on the difference curvature.

3. Adaptive TV model

Based on the difference curvature, the ATV model is presented as follows:

$$E_{ATV} = \int_{\Omega} \left(|\nabla u|^{p(D)} + \frac{1}{2}\lambda(D)(u-u_0)^2 \right) dx\,dy \tag{6}$$

where the functions $p(D)$ and $\lambda(D)$ are

$$p(D) = 2 - \sqrt{\overline{D}} \tag{7}$$

$$\lambda(D) = k \cdot \sqrt{\overline{D}} \tag{8}$$

where k is a positive constant parameter, and $\overline{D}$ is the normalized difference curvature $\overline{D} = \frac{D}{D_{\max}}$, where $D_{\max}$ is the maximal value of difference curvature D across the entire image.

Because $\overline{D} \in [0,1]$, the function $p(D) : \Re^+ \to [1,2]$ monotonically decreases from 2 to 1, and the function $\lambda(D) \in [0,k]$. At sharp edges, $p(D) \to 1$ and $\lambda(D) \to k$. In flat and ramp regions and for isolated noise, $p(D) \to 2$ and $\lambda(D) \to 0$. According to the behavioral analysis of the difference curvature D, we can observe that the ATV model automatically adapts the gradient exponent and the weight of the fidelity term to fit the data and preserve the fine details, respectively. The regularization term is approximate to the TV norm and the weight of the fidelity term is large near edges, while the regularization term is approximate to the L2 norm and the weight of the fidelity term is small away from the edges. Therefore the ATV model can preserve edges and fine details, and prevent staircasing.

Using the steepest descent method, we obtain the steady state of our model (6):

$$\partial_t u = \mathrm{div}(g(|\nabla u|)\nabla u) + \lambda(D)(u_0 - u), \Omega \times [0,\infty) \tag{9}$$

Here, $u(0) = u_0$ and the diffusivity $g(s) = \phi'(s)/s$ with the variational penalty function $\phi(s) = s^{p(D)}$. The diffusion properties of our model

Table 4
SNR results of Fig. 7 (unit: db).

Figures	7(b)	7(c)	7(d)	7(e)	7(f)	7(g)	7(h)	7(i)	7(j)
SNR	12.411	15.355	14.339	14.173	12.025	13.045	15.199	15.057	14.270
Figures	7(k)	7(l)	7(m)	7(n)	7(o)	7(p)	7(q)	7(r)	7(s)
SNR	15.594	14.374	16.238	15.636	16.252	16.478	15.051	16.365	16.231

Table 5
Mean structural similarity (MSSIM) of Fig. 7. The MSSIM is between 0 and 1 with a score of 1 being given only if the denoised image is exactly equivalent to the original image.

Figures	7(b)	7(c)	7(d)	7(e)	7(f)	7(g)	7(h)	7(i)	7(j)
MSSIM	0.6035	0.8218	0.7801	0.7664	0.7275	0.7743	0.8109	0.8175	0.8139
Figures	7(k)	7(l)	7(m)	7(n)	7(o)	7(p)	7(q)	7(r)	7(s)
MSSIM	0.7717	0.7024	0.7878	0.8295	0.8505	0.8509	0.8039	0.8534	0.8515

can be further elucidated by the orthogonal decomposition of Eq. (9) as follows:

$$\partial_t u = \phi''(|\nabla u|)u_{\eta\eta} + g(|\nabla u|)u_{\xi\xi} + \lambda(D)(u_0 - u) \tag{10}$$

Thus, with respect to level sets of u, the first term captures normal diffusion and the second captures tangential diffusion. Therefore, diffusion normal to level sets of u is forward where $\phi'' > 0$ and it is backward where $\phi'' < 0$. For our model, $\phi''(|\nabla u|) = p(D)(p(D)-1)|\nabla u|^{p(D)-2}$ and $g(|\nabla u|) = p(D)|\nabla u|^{p(D)-2}$. Because $\phi'' > 0$ with $p(D) \in [1,2]$, ϕ is a convex function. In our model, ϕ'' is strictly positive for gradient magnitudes corresponding to gradual image variations, i.e. for ramp regions. This leads to much smoother reconstructions in regions of moderate gradient and thus prevents staircasing.

For the measure of convergency, the "normalized step difference energy" (NSDE) [26] was calculated for each iteration: NSDE $= \frac{|u_k - u_{k-1}|^2}{|u_k|^2}$, where u_k and u_{k-1} denote the image vector at the ks and $k-1$s iteration, respectively. Fig. 5 shows the denoising result of the Elaine image. Figs. 5(a) and (b) are the original image and denoising result, respectively. Fig. 5(c) shows the graph of the NSDE of our model. Here, the difference curvature is computed on the noisy image. In the next section, we will analyze the effect of the noise on the difference curvature and denoising results. Fig. 5(c) demonstrates that our model has a convergence.

4. Experimental results and analysis

In this section we first report comparative smoothing results with several denoising methods for a synthesis image. Then we

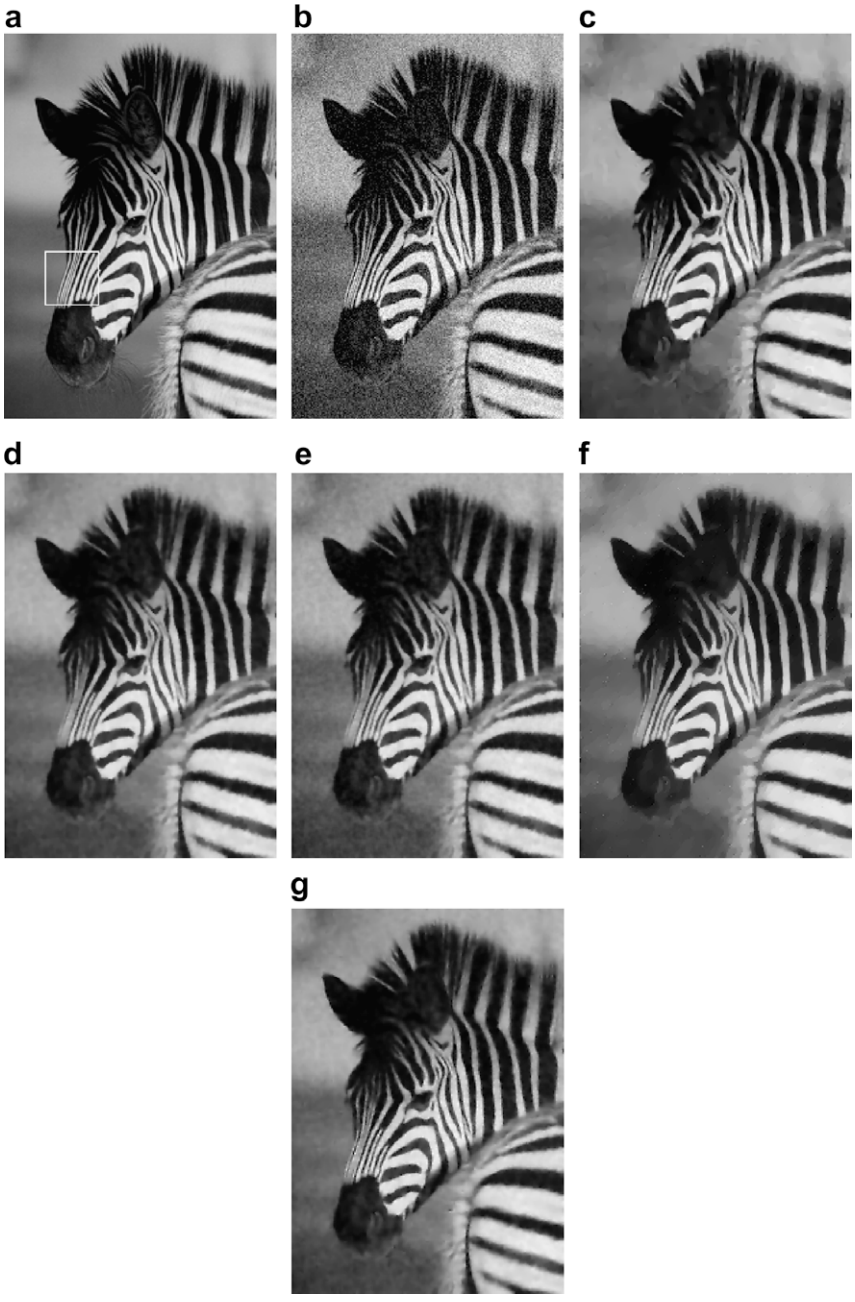

Fig. 8. Comparison of the effect on a zebra image. (a) Original image. The white rectangle indicates a region of special interest which will be zoomed in Fig. 7. (b) Noisy image (additive Gaussian white noise, SNR = 11.5 db). (c) Result by the TV model (SNR = 16.1184 db). (d) Result by the EFG scale filtering (SNR = 15.0665 db). (e) Result by the Gauss-TV filtering (SNR = 15.2708 db). (f) TV2&4 filter (SNR = 14.5879 db). (g) ATV model (SNR = 15.5079 db, iteration = 50, dt = 0.02 (time step), k = 2).

analyze the performance of our model and other total variation based models. Finally, our model is used for the denoising of medical images.

4.1. Comparative results

Fig. 6 shows the comparison of some denoising methods on a synthetic image. Table 2 shows the signal-to-noise ratio (SNR) results of Fig. 6. Table 3 shows the mean structural similarity (MSSIM) [27]. Fig. 6(a) is the original image, and Fig. 6(b) is the noisy image with Gaussian noise. Figs. 6(c)–(r) show the denoising results with the bilateral filtering [28], Gauss curvature-driven diffusion (GCDD) [26], Perona–Malik (PM) model [5], nonlinear complex diffusion [11], adaptive smoothing [29], nonlocal means (NL-means) [30], linear regression neighborhood filter (LYNF) [31], robust anisotropic diffusion [8], adaptive TV method [2], fourth-order PDEs [10], TV method [1], combined model of TV filter and fourth-order PDEs (TV2&4) filter [23], edge-flat-grey (EFG) scale filtering [24], Gauss-TV filtering [25], nonlinear diffusion filtering with an additive operator splitting (AOS) scheme [32], and ATV model, respectively. Fig. 6(s) shows the denoising result with ATV model where the difference curvature is estimated on the pre-denoised image by using the classical TV model. Because some parameters need to be set for each method, the denoising results in Fig. 6 are relatively good, not the best.

From Fig. 6 and Tables 2 and 3, we can observe that (1) Small-scaled features cannot be preserved for the adaptive smoothing, LYNF, TV method and EFG. (2) The denoising capabilities of the GCCD, robust anisotropic and Gauss-TV filtering are not very good, and the noise in the texture region will be preserved for the adaptive TV method. (3) The loss of contrast is obvious for the nonlinear complex diffusion, adaptive smoothing and LYNF. (4) Speckles arise in the fourth-order PDEs. (5) Staircase effect exists in the PM model, adaptive smoothing, adaptive TV method, TV method, TV2&4, and nonlinear diffusion filtering. (6) The denoising result of the NL-means is very good, but its computational cost is very expensive and is similar to the adaptive smoothing. In order to accelerate the NL-means, Wang et al. [33] presented a fast non-local algorithm by exploiting summed square image and fast Fourier transform. (7) MSSIM values indicate that the adaptive TV, nonlinear diffusion filtering and our model can preserve the local structures of the original image well. (8) The denoising capability and the local structure preserving capability of our method can be improved when the difference curvature is computed on the pre-denoised image. (9) Comparing with other denoising methods, our ATV model has a good performance overall, which can preserve important structures, such as edges, ramps, corners and small-scaled features.

Fig. 7 shows the comparison of some denoising methods on a natural image. Tables 4 and 5 show the signal-to-noise ratio and the mean structural similarity of Fig. 7, respectively. Comparing with the synthetic image denoising results (Fig. 6), our model and the total variation based filters with convex variational penalty functions, such as the EFG and Gauss-TV filtering, are better for the natural image. The denoising results of Figs. 7(r) and (s) are similar. Thus the computation of the difference curvature on the pre-denoised image can improve the denoising result when the noise level is high, and has a little effect when the noise level is low.

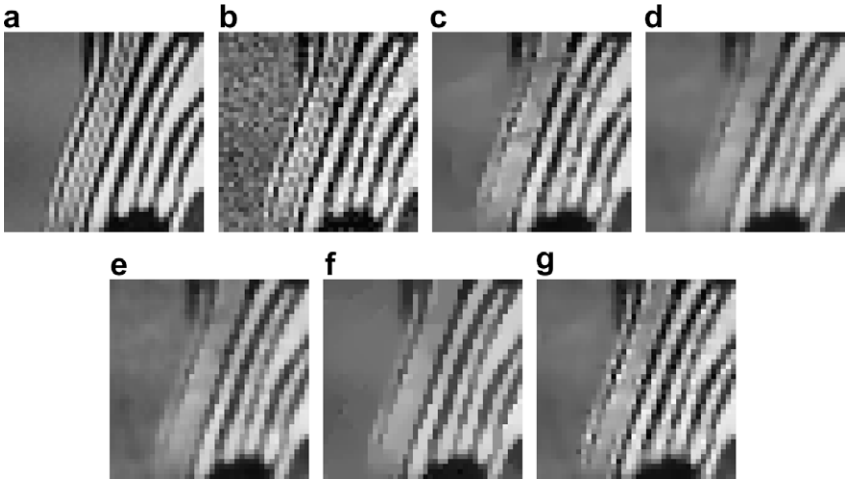

Fig. 9. A small part of zebra image is emphasized to compare the performance of the five models when processing with details. (a) Original image. (b) Noisy image. (c) TV. (d) EFG. (e) Gauss-TV. (f) TV2&4. (g) ATV.

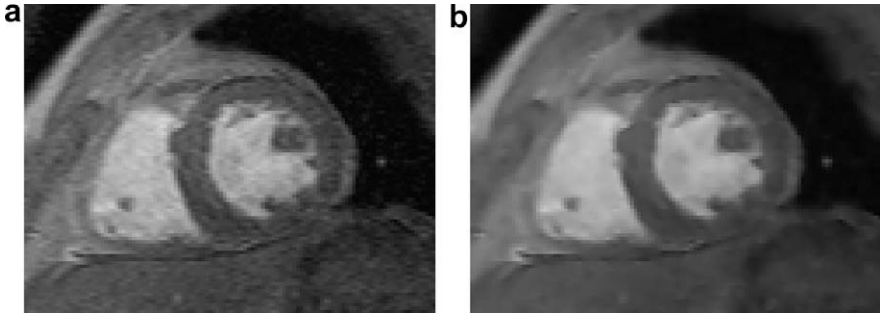

Fig. 10. Denoising results of a left ventricle MR image. (a) Original image. (b) ATV.

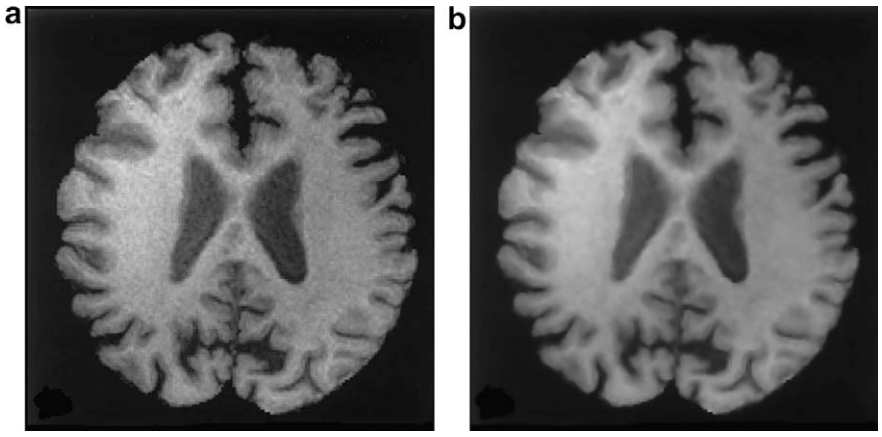

Fig. 11. Denoising results of a brain MR image. (a) Original image. (b) ATV.

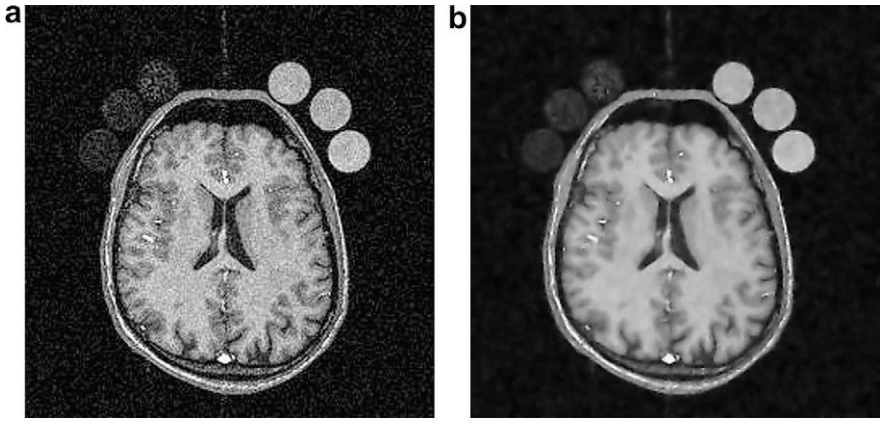

Fig. 12. Denoising results of another brain MR image. (a) Original image. (b) ATV.

Fig. 8 shows the comparison of several total variation based methods on a zebra image of size 283×200. Fig. 8 indicates that the TV model has the staircase effect and the TV2&4 filter also has a little staircase effect. The Gauss-TV filter preserves a realistic roundedness in objects, but also partially preserves the stippled noise pattern in flat regions. Our model performs better than the other total variation based methods to preserve fine details, which is demonstrated in Fig. 9.

4.2. Medical image denoising

In medical image analysis, denoising is the preprocessing of the other steps, such as segmentation and reconstruction. Figs. 10–12 show the denoising of a left ventricle magnetic resonance (MR) image and two brain MR images, respectively. The parameters of our models are as follows: $k = 2$ and dt (time step) is 0.02. Figs. 10–12 indicate that our model can preserve both important structures, such as edges, ramps and small-scaled features, so our model is a good candidate for segmentation preprocessing.

5. Conclusions

In this paper we have developed a new edge indicator, named difference curvature, which can effectively distinguish between edges and ramps. Based on this new indicator, we proposed an adaptive TV models with adaptive regularization and fidelity terms. We tested our models on both synthetic and natural images, and experimental results demonstrate that our model is capable of preserving edges and ramps without smoothing out important fine details.

Acknowledgments

Work was supported by the National Science Foundation of China under grant Nos. 60805003/60773172, and the Postdoctoral Science Foundation of Jiangsu Province under Grant No. AD41158. This research was also supported by a grant from the Research Grants Council of the Hong Kong Special Administrative Region, (Project No. CUHK4121/08E). This work is affiliated with the Virtual Reality, Visualization and Imaging Research Centre at the Chinese University of Hong Kong as well as the CUHK MoE-Microsoft Key Laboratory of Human-Centric Computing and Interface Technologies.

References

[1] L.I. Rudin, S. Osher, E. Fatemi, Nonlinear total variation based noise removal algorithms, Physica D 60 (1992) 259–268.
[2] G. Gilboa, Y.Y. Zeevi, N. Sochen, Texture preserving variational denoising using an adaptive fidelity term, in: Proceedings of the VLSM, Nice, France, 2003, pp. 137–144.
[3] P. Blomgren, T.F. Chan, P. Mulet, Extensions to total variation denoising, in: Proceedings of SPIE, San Diego, vol. 3162, 1997.
[4] T. Chan, A. Marquina, P. Mulet, High order total variation-based image restoration, SIAM Journal on Scientific Computing 22 (2) (2000) 503–516.
[5] P. Perona, J. Malik, Scale-space and edge detection using anisotropic diffusion, IEEE Transactions on Pattern Analysis and Machines Intelligence 12 (7) (1990) 629–639.

[6] L. Alvarez, P.L. Lions, J.M. Morel, Image selective smoothing and edge detection by nonlinear diffusion, SIAM Journal on Numerical Analysis 29 (3) (1992) 845–866.
[7] Y.L. You, W. Xu, A. Tannenbaum, M. Kaveh, Behavioral analysis of anisotropic diffusion in image processing, IEEE Transactions on Image Processing 5 (11) (1996).
[8] M.J. Black, G. Sapiro, D.H. Marimont, D. Heeger, Robust anisotropic diffusion, IEEE Transactions on Image Processing 7 (3) (1998).
[9] H.G. Luo, L.M. Zhu, H. Ding, Coupled anisotropic diffusion for image selective smoothing, Signal Processing 86 (7) (2006) 1728–1736.
[10] Y.L. You, M. Kaveh, Fourth-order partial differential equations for noise removal, IEEE Transactions on Image Processing 9 (10) (2000) 1723–1730.
[11] G. Gilboa, N. Sochen, Y.Y. Zeevi, Image enhancement and denoising by complex diffusion processes, IEEE Transactions on Pattern Analysis and Machines Intelligence 26 (8) (2004) 1020–1036.
[12] T. Chan, S. Esedoglu, F. Park, A. Yip, Recent developments in total variation image restoration, in: N. Paragios, Y. Chen, O. Faugeras (Eds.), Handbook of Mathematical Models in Computer Vision, Springer, Berlin, 2004.
[13] S. Osher, M. Burger, D. Goldfarb, J. Xu, W. Yin, An iterative regularization method for total variation based on image restoration, Multiscale Modeling and Simulation 4 (2) (2005) 460–489.
[14] M. Nikolova, Minimizers of cost-functions involving nonsmooth data-fidelity terms, SIAM Journal on Numerical Analysis 40 (3) (2002) 965–994.
[15] T. Chan, S. Esedoglu, Aspects of total variation regularized L1 function approximation, SIAM Journal of Applied Mathematics 65 (5) (2005) 1817–1837.
[16] S. Esedoglu, S. Osher, Decomposition of images by the anisotropic Rudin–Osher–Fatemi model, Communications in Pure and Applied Mathematics 57 (12) (2004) 1609–1626.
[17] P. Blomgren, P. Mulet, T. Chan, C. Wong, Total variation image restoration: numerical methods and extensions, in: ICIP, Santa Barbara, 1997, pp. 384–387.
[18] C.A. Bouman, K.D. Sauer, A generalized Gaussian image model for edge-preserving MAP estimation, IEEE Transactions on Image Processing 2 (3) (1993) 296–310.
[19] A. Chambolle, P. Lions, Image recovery via total variation minimization and related problems, Numerical Mathematics 76 (2) (1997) 167–188.
[20] M. Lysaker, A. Lundervold, X.C. Tai, Noise removal using fourth-order partial differential equation with applications to medical magnetic resonance images in space and time, IEEE Transactions on Image Processing 12 (12) (2003) 1579–1590.
[21] S. Osher, A. Sole, L. Vese, Image decomposition and restoration using total variation minimization and the H^1 norm, Multiscale Modeling and Simulation 1 (3) (2003) 349–370.
[22] M. Lysaker, X.C. Tai, Iterative image restoration combining total variation minimization and a second-order functional, International Journal of Computer Vision 66 (1) (2006) 5–8.
[23] F. Li, C.M. Shen, J.S. Fan, C.L. Shen, Image restoration combing a total variational filter and a fourth-order filter, Journal of Visual Communication and Image Representation 18 (4) (2007) 322–330.
[24] K. Ito, K. Kunisch, Restoration of edge-flat-grey scale images, Inverse Problems 16 (4) (2000) 909–928.
[25] C. Schnörr, Unique reconstruction of piecewise-smooth images by minimizing strictly convex nonquadratic functionals, Journal of Mathematical Imaging and Vision 4 (1994) 189–198.
[26] S.-H. Lee, J.K. Seo, Noise removal with Gauss curvature-driven diffusion, IEEE Transactions on Image Processing 14 (7) (2005) 904–909.
[27] Z. Wang, A.C. Bovik, H.R. Sheikh, E.P. Simoncelli, Image quality assessment: from error visibility to structural similarity, IEEE Transactions on Image Processing 13 (4) (2004) 600–612.
[28] C. Tomasi, R. Manduchi, Bilateral filtering for gray and color images, in: Proceedings of the IEEE International Conference on Computer Vision, Bombay, India, January 1998, pp. 839–846.
[29] K. Chen, Adaptive smoothing via contextual and local discontinuities, IEEE Transactions on Pattern Analysis and Machines Intelligence 27 (10) (2005) 1552–1567.
[30] A. Buades, B. Coll, J.M. Morel, A nonlocal algorithm for image denoising, in: Proceedings of the IEEE International Conference on Computer Vision Pattern Recognition, vol. 2, June 2005, pp. 60–65.
[31] A. Buades, B. Coll, J.-M. Morel, The staircasing effect in neighborhood filters and its solution, IEEE Transactions on Image Processing 15 (6) (2006) 1499–1505.
[32] J. Weickert, B.M. ter Haar Romeny, M.A. Viergever, Efficient and reliable schemes for nonlinear diffusion filtering, IEEE Transactions on Image Processing 7 (3) (1998) 398–410.
[33] J. Wang, Y.W. Guo, Y.T. Ying, Y.L. Liu, Q.S. Peng, Fast non-local algorithm for image denoising, in: IEEE International Conference on Image Processing, Atlanta, USA, October 2006, pp. 1429–1432.